Orbital Angular Momentum-Entanglement Frequency Transducer

Zhi-Yuan Zhou,[1,2] Shi-Long Liu,[1,2] Yan Li,[1,2] Dong-Sheng Ding,[1,2] Wei Zhang,[1,2] Shuai Shi,[1,2] Ming-Xin Dong,[1,2] Bao-Sen Shi,[1,2,*] and Guang-Can Guo[1,2]

[1]*Key Laboratory of Quantum Information, University of Science and Technology of China, Hefei, Anhui 230026, China*

[2]*Synergetic Innovation Center of Quantum Information & Quantum Physics, University of Science and Technology of China, Hefei, Anhui 230026, China*

(Received 24 March 2016; revised manuscript received 22 May 2016; published 29 August 2016)

Entanglement is a vital resource for realizing many tasks such as teleportation, secure key distribution, metrology, and quantum computations. To effectively build entanglement between different quantum systems and share information between them, a frequency transducer to convert between quantum states of different wavelengths while retaining its quantum features is indispensable. Information encoded in the photon's orbital angular momentum (OAM) degrees of freedom is preferred in harnessing the information-carrying capacity of a single photon because of its unlimited dimensions. A quantum transducer, which operates at wavelengths from 1558.3 to 525 nm for OAM qubits, OAM-polarization hybrid-entangled states, and OAM-entangled states, is reported for the first time. Nonclassical properties and entanglements are demonstrated following the conversion process by performing quantum tomography, interference, and Bell inequality measurements. Our results demonstrate the capability to create an entanglement link between different quantum systems operating in a photon's OAM degrees of freedom, which will be of great importance in building a high-capacity OAM quantum network.

DOI: 10.1103/PhysRevLett.117.103601

Qubits and entanglement are the key resources of quantum communications and computations [1,2]. Different physical systems such as photon pairs [2], trapped ions [3], and cold atomic gases [4] can be used to encode qubit states or generate entanglement. The photon has proved most suitable in transferring information between different systems, such as quantum memory and quantum processors, or along communication channels. For a photonic qubit or an entanglement state, information can be encoded in various degrees of freedoms (DOF); entanglement can be constructed via a photon's polarization [5], in time bins [6], and in orbital angular momentum (OAM) [7]. Among these DOFs of light, its OAM provides unique features, including the mechanical torch effect, and singularities in phase-intensity distributions, which have broad applications in microparticle manipulations [8], high precision optical metrology [9–11], and potential high-capacity information encoding in optical communications [12,13].

Recently, much effort has gone into exploiting OAM light in quantum information technologies. Since the pioneering work demonstrating entanglement in OAM [7], great advances have been made in the experimental control of OAM superposition states and their use in various protocols; they include quantum cryptography [14], the demonstration of very-high-dimensional entanglement [15,16], and quantum teleportation from spin to OAM [17]. More recently, quantum memory for OAM qubits [18,19] and entangled states [20–22] were demonstrated showing the capability for high-density information encoding and processing. A complete high-capacity quantum network operating in the photonic OAM should have some basic components that serve as quantum memory, quantum processors, or communication channels [1]. To realize these components, the underlying physical systems usually work at different wavelengths. Transferring information between these systems effectively requires wavelength bridges which map the frequencies of one photon to another photon while preserving its quantum features.

Such wavelength bridges can be realized using second-order nonlinear processes, in which two optical fields combine in a nonlinear medium to generate a third field [23]. Energy, linear optical momentum, and OAM are conserved in the interaction process. By using high-efficiency quasi-phase-matching nonlinear waveguides, much progress in building a wavelength bridge between various systems has been made. In 2005, Tanzilli *et al.* demonstrated that time-bin entanglement between two photons at 1555 and 1312 nm generated by spontaneous parametric down-conversion (SPDC) was preserved after up-conversion from 1312 to 712.4 nm [24]; in 2010, Rakher *et al.* verified that a single telecom-band photon at 1.3 μm generated from a quantum dot can be up-converted to 710 nm [25]; in 2011, Ikuta *et al.* showed down-conversion for a polarization-entangled photon from 780 to 1522 nm [26]; in 2014, Vollmer *et al.* demonstrated up-conversion of a 1550-nm squeezed vacuum state to 532 nm [27]. Recent progress in up-conversion detectors allows photon detection using high-performance visible optical detectors, although in each case the light detected is a highly attenuated laser [28]. We find that the spatial modes used are fundamental

Gaussian modes because nonlinear waveguides supporting a high-order spatial mode are still unobtainable. Until recently, quantum frequency conversion (QFC) of OAM quantum states had been an open problem. We demonstrated the up-conversion of heralded 1560-nm single-photon OAM states to 525 nm [29]. Because an OAM entanglement state has the capability to realize more sophisticated applications in quantum information science that cannot be accomplished using single-photon OAM states, the QFC of an OAM-entangled state would be an important step.

We move towards this step by successively up-converting 1558.3-nm OAM qubits, OAM-polarization hybrid-entangled states, and OAM entanglement states to 525 nm. With more advanced experimental techniques compared with those used in Ref. [29], and by performing quantum state tomography (QST), two-photon interference, and Bell-Clauser-Horne-Shimony-Holt (Bell-CHSH) inequality measurements, we clearly show that the quantum superposition and entanglement of the states are retained after up-conversion.

QFC can be accomplished using sum frequency generation (SFG), in which the annihilation of a strong pump photon (ω_p) and a weak signal photon (ω_1) create a SFG photon with frequency ($\omega_2 = \omega_1 + \omega_p$). The effective Hamilton operator for this process is [27,29]

$$\hat{H}_{\text{eff}} = i\hbar\xi(\hat{a}_{1,l}\hat{a}^{\dagger}_{2,l} - \hat{a}^{\dagger}_{1,l}\hat{a}_{2,l}), \tag{1}$$

where $\hat{a}_{1,l}$ and $\hat{a}^{\dagger}_{2,l}$ represent, respectively, the annihilation and creation operators of the signal and SFG photons; l denotes the OAM index of the signal and SFG photons—because of OAM conservation in the SFG process, the signal photon's OAM is linearly transferred to the SFG process; and ξ is a constant, which is proportional to the product of the pump amplitude E_p and the second-order susceptibility $\chi^{(2)}$. The evolution of $\hat{a}_{j,l}$ obtained in the Heisenberg picture is given as

$$\hat{a}_{1,l}(t) = \hat{a}_{1,l}(0)\cos(\xi t) - \hat{a}_{2,l}(0)\sin(\xi t), \tag{2}$$

$$\hat{a}_{2,l}(t) = \hat{a}_{2,l}(0)\cos(\xi t) + \hat{a}_{1,l}(0)\sin(\xi t). \tag{3}$$

When $\xi t_f = \pi/2$, the input signal field is completely converted to the output SFG field $\hat{a}_{2,l}(t_f) = \hat{a}_{1,l}(0)$. As ξ strongly depends on the pump amplitude, the key point for reaching maximum conversion efficiency is to increase the pump power. In this Letter, the conversion efficiency is increased using a ring cavity to enhance the pump power.

Up-conversion of OAM qubit states is investigated next. The 1558.3-nm photon source used in the experiments is generated using SPDC with a type-II periodically poled potassium titanyl phosphate (PPKTP) crystal in a Sagnac-loop configuration (see the Supplemental Material for Ref. [30]). The Sagnac loop is operated in a single circulation direction by rotating the wave plates of the pump beam. The OAM qubits are generated using a modified Sagnac loop with a vortex phase plate (VPP) placed in the loop [29,31,32] (see the mode converter in Fig. 1). The function of the mode converter is to generate OAM qubit states

$$\alpha|l\rangle + \beta|-l\rangle, \tag{4}$$

where $|\alpha|^2 + |\beta|^2 = 1$, and α and β depend on the positions of the (half and quarter) wave plates (HWP, QWP) in the input ports of the mode converter; l is the photon's topological charge generated with VPP. Although $l = 1$ is used in all experiments, all experimental results can be extended to other l values. For convenience, we denote the qubit basis by $|R\rangle = |l\rangle$ and $|L\rangle = |-l\rangle$. We characterize the performance of our up-conversion device by converting a set of qubit states distributed over the Bloch sphere and subsequently performing QST on the up-converted states. Reconstructing the density matrix $\hat{\rho}$ of any two-dimensional states requires the measurement of four Stokes parameters that appear in the expansion [33]

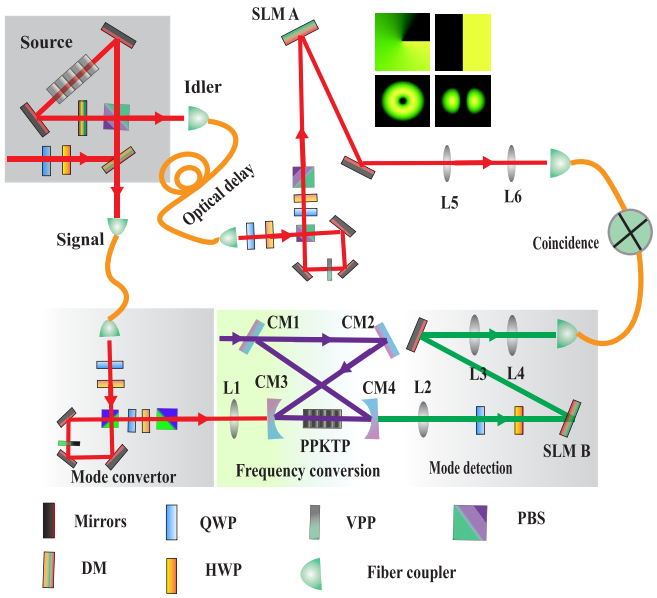

FIG. 1. Schematic of the experimental setup. The Sagnac loop is operated in a single circulation direction to generate degenerate orthogonally polarized photon pairs at 1558.3 nm. The mode converter can be used to encode arbitrary qubit states or for converting entanglement type from polarization to OAM. The frequency conversion is performed in a ring cavity, which is pumped at 791.0 nm. The mode detection for idler (signal) photon is performed using SLM A (B) (HOLOEYE, LETO, 1920 × 1080 resolution; SLM A, 8-μm pixel pitch, and SLM B, 6.4-μm pixel pitch). The frequency up-converted signal photon and idler photon are detected by InGaAs and Si-avalanched single-photon detectors, and subsequently, coincidence measurements are performed (Timeharp 260, Pico Quanta, 1.6-ns coincidence window). CM: cavity mirror; DM: dichromatic mirror.

$$\hat{\rho} = \frac{1}{2}\sum_{i=0}^{3}\frac{S_i}{S_0}\hat{\sigma}_i, \tag{5}$$

where $\hat{\sigma}_0$ is the identity matrix and $\hat{\sigma}_i$ $(i = 1, 2, 3)$ are the Pauli spin operators. To evaluate the coefficient S_i, projection measurements are performed on the four basis vectors ($|R\rangle$, $|L\rangle$, $|H\rangle$, $|A\rangle$), where basis vectors $|R\rangle$, $|L\rangle$ are defined in the context above; $|H\rangle$, $|A\rangle$ are defined as $|H\rangle = 1/\sqrt{2}(|R\rangle + |L\rangle)$,$|A\rangle = 1/\sqrt{2}(|R\rangle - i|L\rangle)$, respectively. The other two basis vectors used in experiments are $|V\rangle = 1/\sqrt{2}(|R\rangle - |L\rangle)$, and $|D\rangle = 1/\sqrt{2}(|R\rangle + i|L\rangle)$. The projection measurements are conducted using a spatial light modulator (SLM), which is calibrated at wavelength 532 nm. By imprinting a phase mask on the SLM with opposite phase content, the spiral phase front of the SFG photon is flattened to a plane wave front that can be effectively coupled to a single-mode fiber (SMF) (see the Supplemental Material for Ref. [30]). Density matrices are reconstructed using the maximum likelihood method from the experimental data. Experimental reconstructed density matrices for the qubit states $|R\rangle$, $|L\rangle$, $|H\rangle$, $|D\rangle$ are shown in Fig. 2; the first column shows their phase and intensity distributions, and the second and third columns give the real and imaginary parts of the qubit states (for comparison, the ideal density matrices are supplied in the Supplemental Material for Ref. [30], Fig. S2). In Table I, we give the fidelities of the four qubit states without (with) dark count coincidence subtracted. The fidelity is defined as $\langle\Phi|\rho|\Phi\rangle$, where $|\Phi\rangle$ is the ideal qubit state. The average fidelity is 0.954 ± 0.016 (0.963 ± 0.012) without (with) the dark count subtracted. The slightly lower fidelity of the $|D\rangle$ state is because of imperfect preparation of the input state. Nevertheless, the high fidelity shows the reliable performance of our up-conversion device and hence paves the way for OAM entanglement states' up-conversion.

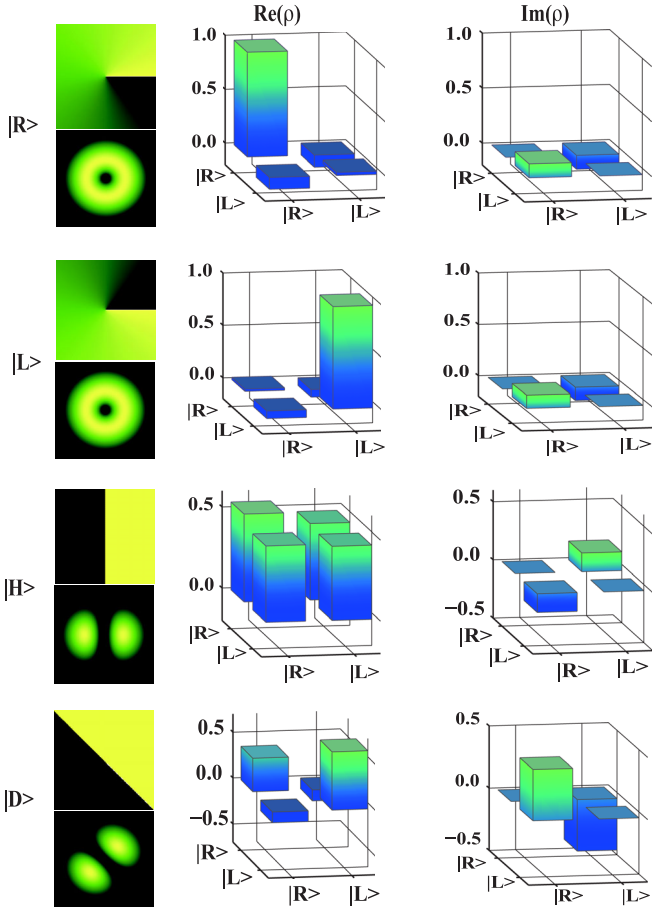

FIG. 2. Reconstructed density matrices for the four qubit states $|R\rangle$, $|L\rangle$, $|H\rangle$, $|D\rangle$. The first column shows the intensity and phase distributions imprinted on SLM A. The second and third columns give the real and imaginary parts of the density matrices. No background correction is applied.

Next, we describe the up-conversion of the OAM-polarization hybrid-entangled state. Hybrid entanglement is generated by mode conversion from a Sagnac-loop-based polarization-entangled source, which can generate entangled states [34,35]

$$|\Phi\rangle^{\pm} = \frac{1}{\sqrt{2}}(|hv\rangle \pm |vh\rangle). \tag{6}$$

By performing mode conversion on one of the photons, the state is transformed to an OAM-polarization hybrid-entangled state of the form [32]

$$|\Phi\rangle_{\text{hybrid}}{}^{\pm} = \frac{1}{\sqrt{2}}(|h, R\rangle \pm |v, L\rangle). \tag{7}$$

Here, the state $|\Phi\rangle^{+}_{\text{hybrid}}$ is used. The 1558.3-nm signal photon in the OAM mode is sent to the frequency conversion module, which is then up-converted to 525 nm. It is subsequently transformed to a Gaussian mode using the mode-detection module and coupled to a SMF. The idler photon is optically delayed with a SMF, and together with the up-converted signal photon, coincidence measurements are made.

To verify that entanglement is preserved during up-conversion, two-photon interference and QST are used to characterize the up-converted state. Two interference fringes are measured when the idler photon is polarized in the diagonal ($|d\rangle$) or right circular ($|r\rangle$) state [Fig. 3(a)]. For each polarization setting, we record coincidences over a 100-s period as a function of the rotation angle of the phase mask applied to SLM B. The definition of the angle is $|\theta\rangle = 1/\sqrt{2}(e^{i\theta}|R\rangle + e^{-i\theta}|L\rangle)$ (see the Supplemental Material for Ref. [30], Fig. S3). The interference visibilities

TABLE I. Fidelities of four qubits in the up-conversion process without and with dark count coincidence subtraction.

Input modes	Raw fidelity	Net fidelity
$\|R\rangle$	0.970 ± 0.007	0.977 ± 0.005
$\|L\rangle$	0.978 ± 0.004	0.982 ± 0.004
$\|H\rangle$	0.952 ± 0.036	0.967 ± 0.023
$\|D\rangle$	0.916 ± 0.015	0.926 ± 0.016

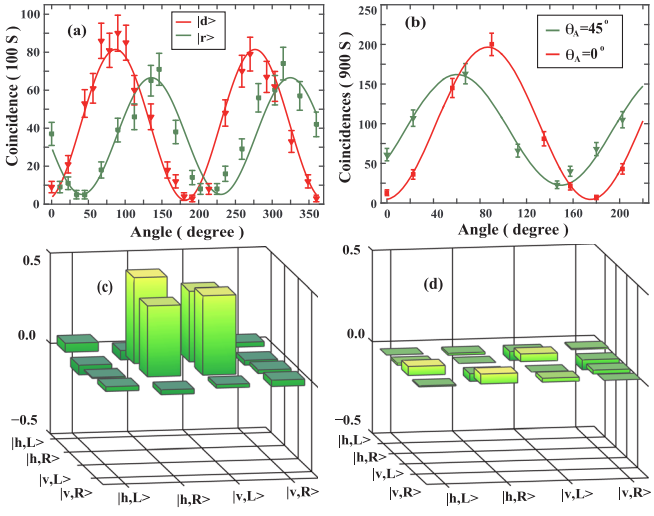

FIG. 3. Two-photon interference fringes for (a) the OAM-polarization hybrid-entangled state and (b) the OAM-entangled state. Uncertainty errors are given assuming a Poisson distribution for the photon statistics. (c),(d) Real and imaginary parts of the reconstructed density matrices for the hybrid-entangled state.

without (with) dark count coincidences subtracted are 0.949 ± 0.029 (0.972 ± 0.027) and 0.856 ± 0.068 (0.907 ± 0.053) for $|d\rangle$ and $|r\rangle$, respectively.

To know precisely what the up-converted state is, one needs to perform QST to reconstruct the density matrix of the state; the result is shown in Figs. 3(c) and 3(d). By comparing with the ideal hybrid state $|\Phi\rangle^{+}_{\text{hybrid}}$, the fidelity of the up-conversion ${}^{+}_{\text{hybrid}}\langle\Phi|\rho|\Phi\rangle^{+}_{\text{hybrid}}$ is 0.837 ± 0.025 (0.861 ± 0.036) without (with) dark count coincidence subtracted. The data acquisition time for QST is 200 s. The uncertainty errors are estimated by assuming a Poisson distribution for the photon statistics. From the reconstructed density matrix, we can deduce the concurrence C of the hybrid-entanglement state [36], which is 0.719 ± 0.033 (0.743 ± 0.047) without (with) dark count coincidence subtracted; $C > 0$ clearly indicates the survival of the entanglement after frequency transducing.

Finally, we describe the up-conversion of an OAM-entangled state. When the idler photon is also transformed with the mode converter, the polarization-entangled state is transformed to an OAM-entangled state [31]

$$\Phi_{\text{OAM}}{}^{\pm} = \frac{1}{\sqrt{2}}(|R,L\rangle \pm |L,R\rangle). \tag{8}$$

Here, the state $|\Phi\rangle^{-}_{\text{OAM}}$ is used. The signal photon undergoes the same procedures as described in the previous section. The idler photon is passed through a delay SMF, mode converter, and mode-detection module. Finally, a coincidence measurement between the idler photon and the up-converted signal photon is performed. To demonstrate entanglement is preserved during up-conversion, we measured the two-photon interference fringes first [Fig. 3(b)]. Coincidences over a 900-s period are recorded as a function of the rotation angle of the phase mask applied to SLM B when the angle of the phase mask in SLM A is set at 0° and 45°. The visibilities for the 0° and 45° bases without (with) dark count coincidences subtracted are 0.955 ± 0.023 (0.994 ± 0.008) and 0.750 ± 0.062 (0.784 ± 0.059), respectively. Visibilities greater than 71% indicate possible violation of the Bell inequality, which implies the presence of entanglement.

To further characterize the entanglement property of the up-converted state, we check the S parameter of the Bell-CHSH inequality defined as [37]

$$S = E(\theta_A,\theta_B) - E(\theta_A,\theta'_B) + E(\theta'_A,\theta_B) + E(\theta'_A,\theta'_B), \tag{9}$$

where $E(\theta_A,\theta_B)$ is expressed as

$$E(\theta_A,\theta_B) = \frac{C(\theta_A,\theta_B) + C(\theta_A+\pi/2,\theta_B+\pi/2) - C(\theta_A+\pi/2,\theta_B) - C(\theta_A,\theta_B+\pi/2)}{C(\theta_A,\theta_B) + C(\theta_A+\pi/2,\theta_B+\pi/2) + C(\theta_A+\pi/2,\theta_B) + C(\theta_A,\theta_B+\pi/2)}. \tag{10}$$

The settings for the four angles are $\theta_A = 0$ and $\theta_B = \pi/8, \theta'_A = \pi/4$ and $\theta'_B = 3\pi/8$. For classical correlations, $|S| \le 2$. Our measurements give an S value of 2.39 ± 0.12 (2.50 ± 0.09) without (with) dark count coincidence subtracted, which violates the inequality by more than 3 standard deviations. Thus, we have strong evidence for the presence of entanglement after frequency up-conversion.

We have described a quantum frequency transducer for OAM qubits, OAM-polarization hybrid-entangled states, and OAM-entangled states enabling conversions from 1558.3 to 525 nm. Our results answer basic questions concerning the QFC of OAM states: Is it possible to convert OAM entanglement from one wavelength to another wavelength? Do superpositions of OAM states and entanglements survive after QFC? Our demonstrations give positive answers to these questions. Nevertheless, there are other important issues that need to be solved. One is the quantum efficiency during conversion; another is how to increase the dimensions of the states for conversion. Feasible resolutions of these issues are given in the following.

In theory, there is no limitation in increasing the conversion efficiency to unity. For increasing the overall quantum conversion efficiencies, first the bandwidth of the photon source for conversion should match the bandwidth of the SFG crystal. In this Letter, the quantum efficiency is 0.01 for a coherent narrow bandwidth laser and is 0.002 for

the signal photon because only 20% of the photons are in the effective bandwidth of the SFG crystal. This problem can be solved by using a longer crystal in SPDC to generate photon pairs and a shorter crystal for QFC. The key point in increasing conversion efficiency is to increase the pump power. For up-conversion of continuous-wave photons, one needs to optimize the cavity loss and the transmittance of the input coupling mirror, and a high-intensity pump laser is needed. For pulsed photons, a high-intensity laser is also preferred in achieving high conversion efficiency. Researchers have already realized high conversion efficiency for lower-order OAM modes in the pulsed regime using an attenuated laser source [38].

Regarding dimensions in QFC, the physical limitations of the dimensions are the crystal thickness and beam waist of the strong pump beam. The thickness of the crystal used in this experiment is 1 mm, as the OAM beam size w_l scales with l in $w_l = \sqrt{l+1}w_0$, where w_0 is the beam waist of the Gaussian beam. The crystal can support up to 1200 modes for $w_0 = 20$ μm. If the pump beam waist is limited to 100 μm, at least 49 OAM modes are effectively overlapped with the pump beams. In the classical optical regime, $l = 100$ is obtained in second harmonic generation [39]. In our experiments, the $l = 1$ mode is used only as an example. If the conversion efficiency issue is solved, dimensional limitations on l pose no problem.

In conclusion, the experiments described above provide a first look at frequency up-conversions of an OAM qubit, an OAM-polarization hybrid-entangled state, and an OAM-entangled state. Various measurements, including QST, interference, and the Bell-CHSH inequality, were used to characterize the performance of the frequency converter for the various quantum states. Preservation of quantum superposition and entanglement survival demonstrate the quantum nature of the conversion. The results open doors for new research into QFC in the photon's OAM, which will stimulate broad interest in solving the remaining issues discussed above. Up-conversion of the OAM of a photon enables a quantum wavelength bridge that links two quantum systems that can be exploited in future high-capacity quantum networks.

We thank Dr. Robert Fickler for helpful discussions. This work was supported by the National Fundamental Research Program of China (Grant No. 2011CBA00200), the National Natural Science Foundation of China (Grants No. 11174271, No. 61275115, No. 61435011, and No. 61525504), and the Fundamental Research Funds for the Central Universities.

*Corresponding author.
drshi@ustc.edu.cn

[1] H. J. Kimble, Nature (London) **453**, 1023 (2008).
[2] A. I. Lvovsky, B. C. Sanders, and W. Tittel, Nat. Photonics **3**, 706 (2009).
[3] B. B. Blinov, D. L. Moehring, L.-M. Duan, and C. Monroe, Nature (London) **428**, 153 (2004).
[4] D. N. Matsukevich and A. Kuzmich, Science **306**, 663 (2004).
[5] P. G. Kwait, K. Mattle, H. Weinfurter, A. Zeilinger, A. V. Sergienko, and Y. Shih, Phys. Rev. Lett. **75**, 4337 (1995).
[6] I. Marcikic, H. de Riedmatten, W. Tittel, V. Scarani, H. Zbinden, and N. Gisin, Phys. Rev. A **66**, 062308 (2002).
[7] A. Mair, A. Vaziri, Gregor Weihs, and A. Zeilinger, Nature (London) **412**, 313 (2001).
[8] D. G. Grier, Nature (London) **424**, 810 (2003).
[9] M. P. J. Lavery, F. C. Speirits, S. M. Barnett, and M. J. Padgett, Science **341**, 537 (2013).
[10] V. D'Ambrosio, N. Spagnolo, L. D. Re, S. Slussarenko, Y. Li, L. C. Kwek, L. Marrucci, S. P. Walborn, L. Aolita, and F. Sciarrino, Nat. Commun. **4**, 2432 (2013).
[11] Z.-Y. Zhou, Y. Li, D.-S. Ding, W. Zhang, S. Shi, and B.-S. Shi, Opt. Lett. **39**, 5098 (2014).
[12] J. Wang, J.-Y. Yang, I. M. Fazal, N. Ahmed, Y. Yan, H. Huang, Y. Ren, Y. Yue, S. Dolinar, M. Tur, and A. E. Willner, Nat. Photonics **6**, 488 (2012).
[13] N. Bozinovic, Y. Yue, Y. Ren, M. Tur, P. Kristensen, H. Huang, A. E. Willner, and S. Ramachandran, Science **340**, 1545 (2013).
[14] G. Vallone, V. D'Ambrosio, A. Sponselli, S. Slussarenko, L. Marrucci, F. Sciarrino, and P. Villoresi, Phys. Rev. Lett. **113**, 060503 (2014).
[15] A. C. Dada, J. Leach, G. S. Buller, M. J. Padgett, and E. Andersson, Nat. Phys. **7**, 677 (2011).
[16] M. Krenn, M. Huber, R. Fickler, R. Lapkiewicz, S. Ramelow, and A. Zeilinger, Proc. Natl. Acad. Sci. U.S.A. **111**, 6243 (2014).
[17] X.-L. Wang, X.-D. Cai, Z.-E. Su, M.-C. Chen, D. Wu, L. Li, N.-L. Liu, C.-Y. Lu, and J.-W. Pan, Nature (London) **518**, 516 (2015).
[18] D.-S. Ding, Z.-Y. Zhou, B.-S. Shi, and G.-C. Guo, Nat. Commun. **4**, 2527 (2013).
[19] A. Nicolas, L. Veissier, L. Giner, E. Giacobino, D. Maxein, and J. Laurat, Nat. Photonics **8**, 234 (2014).
[20] D.-S. Ding, W. Zhang, Z.-Y. Zhou, S. Shi, G.-Y. Xiang, X.-S. Wang, Y.-K. Jiang, B.-S. Shi, and G.-C. Guo, Phys. Rev. Lett. **114**, 050502 (2015).
[21] Z.-Q. Zhou, Y.-L. Hua, X. Liu, G. Chen, J.-S. Xu, Y.-J. Han, C.-F. Li, and G.-C. Guo, Phys. Rev. Lett. **115**, 070502 (2015).
[22] D.-S. Ding, W. Zhang, S. Shi, Z.-Y. Zhou, Y. Li, B.-S. Shi, and G.-C. Guo, Light Sci. Appl. (to be published).
[23] G. D. Boyd and D. A. Kleinman, J. Appl. Phys. **39**, 3597 (1968).
[24] S. Tanzilli, W. Tittel, M. Halder, O. Alibart, P. Baldi, N. Gisin, and H. Zbinden, Nature (London) **437**, 116 (2005).
[25] M. T. Rakher, L. Ma, O. Slattery, X. Tang, and K. Srinivasan, Nat. Photonics **4**, 786 (2010).
[26] R. Ikuta, Y. Kusaka, T. Kitano, H. Kato, T. Yamamoto, M. Koashi, and N. Imoto, Nat. Commun. **2**, 537 (2011).
[27] C. E. Vollmer, C. Baune, A. Samblowski, T. Eberle, V. Händchen, J. Fiurášek, and R. Schnabel, Phys. Rev. Lett. **112**, 073602 (2014).

[28] G.-L. Shentu, J. S. Pelc, X.-D. Wang, Q.-C. Sun, M.-Y. Zheng, M. M. Fejer, Q. Zhang, and J.-W. Pan, Opt. Express **21**, 13986 (2013).

[29] Z.-Y. Zhou, Y. Li, D.-S. Ding, W. Zhang, S. Shi, B.-S. Shi, and G.-C. Guo, Light Sci. Appl. **5**, e16019 (2016).

[30] See Supplemental Material at http://link.aps.org/supplemental/10.1103/PhysRevLett.117.103601 for details of the experimental parameters and data processing method.

[31] R. Fickler, R. Lapkiewicz, W. N. Plick, M. Krenn, C. Schaeff, S. Ramelow, and A. Zeilinger, Science **338**, 640 (2012).

[32] R. Fickler, M. Krenn, R. Lapkiewicz, S. Ramelow, and A. Zeilinger, Sci. Rep. **3**, 1914 (2013).

[33] D. F. V. James, P. G. Kwiat, W. J. Munro, and A. G. White, Phys. Rev. A **64**, 052312 (2001).

[34] Y. Li, Z.-Y. Zhou, D.-S. Ding, and B.-S. Shi, Opt. Express **23**, 28792 (2015).

[35] A. Fedrizzi, T. Herbst, A. Poppe, T. Jennewein, and A. Zeilinger, Opt. Express **15**, 15377 (2007).

[36] V. Coffman, J. Kundu, and W. K. Wootters, Phys. Rev. A **61**, 052306 (2000).

[37] J. F. Clauser, M. A. Horne, A. Shimony, and R. A. Holt, Phys. Rev. Lett. **23**, 880 (1969).

[38] R. Tang, X. Li, W. Wu, H. Pan, H. Zeng, and E. Wu, Opt. Express **23**, 9796 (2015).

[39] Z.-Y. Zhou, D.-S. Ding, Y.-K. Jiang, Y. Li, S. Shi, X.-S. Wang, and B.-S. Shi, Opt. Express **22**, 20298 (2014).